MNRAS **462,** S459–S467 (2016)
Advance Access publication 2016 December 7
doi:10.1093/mnras/stw3148

Structure and evolution of the diamagnetic cavity at comet 67P/Churyumov–Gerasimenko

C. Goetz,[1]★ C. Koenders,[1] K. C. Hansen,[2] J. Burch,[3] C. Carr,[4] A. Eriksson,[5] D. Frühauff,[1] C. Güttler,[6] P. Henri,[7] H. Nilsson,[8] I. Richter,[1] M. Rubin,[9] H. Sierks,[6] B. Tsurutani,[10] M. Volwerk[11] and K. H. Glassmeier[1,6]

[1]*Institut für Geophysik und extraterrestrische Physik, TU Braunschweig, Mendelssohnstr. 3, D-38106 Braunschweig, Germany*
[2]*Department of Atmospheric, Oceanic and Space Sciences, University of Michigan, 2455 Hayward Street, Ann Arbor, MI 48109, USA*
[3]*Southwest Research Institute, PO Drawer 28510, San Antonio, TX 78228-0510, USA*
[4]*Space and Atmospheric Physics Group, Imperial College London, Exhibition Road, London SW7 2AZ, UK*
[5]*Swedish Institute of Space Physics, Angström Laboratory, Lägerhyddsvägen 1, SE-75105 Uppsala, Sweden*
[6]*Max-Planck-Institut für Sonnensystemforschung, Justus-von-Liebig-Weg 3, D-37077 Göttingen, Germany*
[7]*Laboratoire de Physique et Chimie de l'Environnement et de l'Espace, UMR 7328 CNRS, Université d'Orléans, F-45100 Orléans, France*
[8]*Swedish Institute of Space Physics, PO Box 812, SE-981 28 Kiruna, Sweden*
[9]*Physikalisches Institut, University of Bern, Sidlerstrasse 5, CH-3012 Bern, Switzerland*
[10]*Jet Propulsion Laboratory, California Institute of Technology, 4800 Oak Grove Drive, Pasadena, CA 91109, USA*
[11]*Institut für Weltraumforschung, Österreichische Akademie der Wissenschaften, Schmiedlstr. 6, A-8042 Graz, Austria*

Accepted 2016 December 1. Received 2016 November 25; in original form 2016 June 29

ABSTRACT

The long duration of the *Rosetta* mission allows us to study the evolution of the diamagnetic cavity at comet 67P/Churyumov–Gerasimenko in detail. From 2015 April to 2016 February 665 intervals could be identified where *Rosetta* was located in a zero-magnetic-field region. We study the temporal and spatial distribution of this cavity and its boundary and conclude that the cavity properties depend on the long-term trend of the outgassing rate, but do not respond to transient events at the spacecraft location, such as outbursts or high neutral densities. Using an empirical model of the outgassing rate, we find a functional relationship between the outgassing rate and the distance of the cavity to the nucleus. There is also no indication that this unexpectedly large distance is related to unusual solar wind conditions. Because the deduced shape of the cavity boundary is roughly elliptical on small scales and the distances of the boundary from the nucleus are much larger than expected we conclude that the events observed by *Rosetta* are due to a moving instability of the cavity boundary itself.

Key words: magnetic fields – plasmas – methods: data analysis – comets: individual: 67P.

1 INTRODUCTION

The detection of a diamagnetic cavity at comet 67P/Churyumov–Gerasimenko (67P) in 2015 July by the magnetometer measurements onboard *Rosetta* (Goetz et al. 2016) was the second time a spacecraft has been able to conduct measurements in such a region. The first detection was by the *Giotto* magnetometer experiment at comet 1P/Halley in 1986 (Neubauer et al. 1986; Neubauer 1988). Although *Giotto* was able to confirm the existence of a cavity at an active comet, due to its single pass through the coma, it was not able to study its evolution. A diamagnetic cavity has also been observed by the Active Magnetospheric Particle Tracer Explorers (AMPTE) artificial comet mission (Haerendel et al. 1986; Luehr, Kloecker & Acuna 1988). Here, barium and lithium were released from a spacecraft and the reaction of the resulting plasma was monitored by another spacecraft downstream. This was the first time a diamagnetic cavity was created by adding a neutral cloud to a charged fluid. The artificial cavity created in this way represents an example for local cavities as opposed to the global cavity at 1P/Halley. With *Rosetta* we now have the opportunity to study the evolution of the diamagnetic cavity in a cometary environment, while following the comet through perihelion. This allows one to describe its shape, dynamics and long-term evolution.

The diamagnetic cavity is the innermost part of the interaction region of the solar wind with a comet. Using a purely hydrodynamical approach, Biermann, Brosowski & Schmidt (1967) showed that the deceleration of the solar wind due to the incorporation of cometary ions, the so-called mass loading (Tsurutani & Smith 1986; Szegö et al. 2000), would lead to the inward flow stopping somewhere close to the nucleus. Since the comet nucleus itself is not magnetized (Auster et al. 2015), the only source of a magnetic field at the

★ E-mail: c.goetz@tu-bs.de

comet is the interplanetary magnetic field (IMF) carried by the solar wind. This implies that with the inability of most solar wind particles to penetrate the inner cometary regions, the magnetic field is also excluded, and forms a magnetic field-free region, the *diamagnetic cavity* (Haerendel 1987). After the 1P/Halley flyby, Cravens (1987) and Ip & Axford (1987) found that there is a pressure balance between the ion–neutral friction force inside the cavity and the magnetic field outside:

$$-\frac{\partial}{\partial r}\left(\frac{B^2}{2\mu_0}\right) = n_i m_i k_{in} n_n (u_i - u_n), \quad (1)$$

where B is the magnetic field; n_i, m_i and u_i are the number density, mass and velocity of the cometary ions, respectively. k_{in} is the ion–neutral friction coefficient which we set to 1.7×10^{-9} cm^3 s^{-1} (Gombosi et al. 1996). The neutral gas density and velocity are n_n and u_n, respectively. In most cases the ion velocity at the boundary may be neglected as the ions should come to a stop at the boundary. The neutral gas density depends on the outgassing rate Q that gives the number of molecules that leave the nucleus per second and is different for each species. The water outgassing rate of 67P at perihelion (1.24 AU) is roughly 2.5×10^{28} s^{-1} and decreases to 8×10^{26} s^{-1} at 2 AU (Hansen 2016). The exact distance of the boundary from the comet may be calculated if the exact radial profiles of the magnetic field and density are known, but may only be estimated if values at the boundary are given.

Simulations by Koenders et al. (2015) and Rubin et al. (2012) for comet 67P have shown that in steady-state cases the cavity boundary is indeed characterized by this pressure balance. They find that the distance to the nucleus is about 50–100 km depending on the phase angle, the angle between the Sun-comet line and the spacecraft comet line. Four-fluid simulations presented in Huang et al. (2016) show that with an asymmetric outgassing profile the cavity extends to 100 km.

Goetz et al. (2016) reported that the extension of the cavity was much larger than theoretically expected, based on the analysis of magnetic field data during one cavity detection on 2015 July 26. The authors ruled out that an anomalously high neutral gas or dust background was responsible for the extension and showed that the measured outgassing rate combined with a simple model was not high enough either. Instead the authors speculated that the detection of the cavity was due to an instability propagating along the boundary, which increased the distance of the cavity boundary from the nucleus. The particle signatures, especially the electron distribution inside the diamagnetic cavity at 67P was studied by Nemeth et al. (2016) to reveal that there are significant dropouts of electrons in the 100 and 200 eV range.

In this work we investigate 665 detections of the diamagnetic cavity at 67P over the range of 8 months starting late 2015 April at a comet–Sun distance of 1.8 AU and ending 2016 February at a distance of 2.4 AU. We try to extract a general shape of the cavity and aim at a deeper understanding of the dynamics of the cavity boundary.

2 DATA AND METHODS

2.1 Instrumentation

The *Rosetta* spacecraft carries two three-axis fluxgate magnetometers as part of the Rosetta Plasma Consortium (RPC-MAG) with a measurement range of ±16 384 nT and a resolution of 31 pT. The magnetometers have a sampling frequency of 20 vectors s^{-1} (burst mode), which may be downsampled onboard to 1 vector s^{-1} (normal mode) to save data volume (Glassmeier et al. 2007). Although there are two magnetometers mounted on the 1.5 m boom, only the outboard magnetometer is used in this study. The greater distance of the latter from the main spacecraft infrastructure reduces the influence of disturbances related to the spacecraft. The most influential source of magnetic fields on the spacecraft itself are the reaction wheels, but their signature is easily detectable in dynamic spectra in the frequency band of 2–10 Hz. As this publication is concerned only with low frequency phenomena, a low-pass filter with a cut-off of 2 Hz was applied to the high-resolution data, eliminating essentially all effects of the reaction wheels.

Determining the correct offset of a magnetometer in the Solar system is usually a very intricate process, especially if the spacecraft is not spinning, as it is the case with *Rosetta*. The magnetometers on board are influenced by magnetic fields produced on the spacecraft and by a temperature-dependent measurement characteristic. Because of that, the data delivered by the automatic calibration may be influenced by an unknown offset. This is visible in the measurements made in the diamagnetic cavity: even though the magnetic field should be zero in all components, the remaining spacecraft-generated field may reach up to 25 nT. However, during the comet's active phase the magnetic field usually varies on the order of 20 nT min^{-1}, whereas the cavity is still characterized by an absence of turbulence, so it remains easy to detect. Therefore the measurements in the field-free region may be used to construct a new temperature model, spanning from 155 to 210 K, which reduces the remaining field magnitude to below ∼5 nT. This new temperature model may be used any time the magnetometer is in the given temperature range. It should also be noted that the temperature model can be constructed using only a subset of events and predicts the offset for the other events reasonably well. This is another indicator that the field in the diamagnetic cavity region is of the same value for all events. To enable correct analysis, the remaining field in the cavity is removed by taking the individual interval and subtracting the mean of each component. With these data reduction methods, the remaining field in the cavity is reduced to <1 nT. The data calibrated in this way are used for this study.

There are some auxiliary data sets necessary to examine the evolution of the cavity. We use density data from the RPC Mutual Impedance Probe (RPC-MIP; Trotignon et al. 2007) and electron temperature estimates from the RPC Langmuir Probe (RPC-LAP; Eriksson et al. 2007) as well as neutral gas densities from the Rosetta Orbiter Spectrometer for Ion and Neutral Analysis (ROSINA; Balsiger et al. 2007), especially the Comet Pressure Sensor (ROSINA-COPS). To give references with respect to the larger environment around the nucleus we use data from Optical, Spectroscopic, and Infrared Remote Imaging System (OSIRIS; Keller et al. 2007). To gain insight into the solar wind conditions at the comet, we use the simple model developed by Tao et al. (2005) that is available on the Automated Multi-Dataset Analysis (AMDA, amda.cdpp.eu) portal. This model uses OMNI data and a 1D propagation model to extrapolate the solar wind conditions at *Rosetta*. The data are given in the body-centred solar equatorial frame (CSEQ). In this system, the x-axis points towards the Sun and the z-axis is along the part of the solar north pole that is orthogonal to the x-axis. The right-handed coordinate system is completed by the y-axis with the comet at the origin.

During the time period investigated in this study, the trajectory of *Rosetta* was mostly in the terminator plane, meaning *Rosetta* was in a circular orbit along the day–night plane. This configuration is interrupted by a close fly-by in 2015 February and a sudden increase

in distance after a 'safe mode' event in 2015 April. About 1 month after perihelion, the distance was again increased to accommodate a dayside excursion, before going back to a terminator scheme late 2015 October. We have analysed data from 2015 January to 2016 March. No cavity crossings were detected before or after this interval.

2.2 Data analysis procedure

To study the cavity and its boundary we need to be able to identify the intervals of interest. These are clearly distinguishable by sudden decreases in the magnetic field succeeded by an interval where the field is constant and significantly less disturbed than in the surrounding region. We use two methods to find these intervals, one is by hand, and the other is a multistep algorithm. As an example we use data resampled to 1 s. First we apply a low-pass filter with a cut-off frequency of $f_{co} = 100$ mHz. Second we determine all intervals in the data where all magnetic field components are below 10 nT, the numerical derivative is below 0.2 nT s^{-1} and the 10 s-averaged numerical derivative is below 0.1 nT s^{-1}. After choosing only intervals that are longer than 20 s the field in the cavity is compared to the background field in the hour before and after the cavity. Any interval where the background field is not four times higher than the cavity field is discarded. To assure that the cavity can be detected at all times, these values need to be adjusted on a monthly basis due to the changing field characteristics. Obviously this method is heavily dependent on the parameters and even with well-chosen input parameters may not detect some events that are clearly distinguishable by eye. Therefore we chose not to use the automated method to find the intervals instead falling back on the manually selected data set.

For a second level analysis, the temporal extent of the boundary region needs to be determined to allow the study of cavity shape and evolution. This is complicated due to the highly variable magnetic fields in the inner coma, which makes it difficult to distinguish the variations from the boundary proper. This may be seen in the top panel of Fig. 1. We have applied a simple algorithm to determine the cavity boundary. First, we find the most significant (highest field) component of the magnetic field in the 5 min before the cavity. The signal in that component is then low-pass filtered with a cut-off of 0.8 Hz to remove high frequency variations. Then the last peak in the signal before the field decreases to zero is determined. This is assumed to be the end of the boundary region for the inbound pass. The outbound pass is determined in the same fashion.

With the above information, it is also possible to find the vector that is the normal of the boundary plane of the transition region using a minimum variance analysis (MVA; see Sonnerup & Cahill 1967). The method uses the three magnetic field components and computes the direction in which the variance of the field is minimal. This direction then indicates the normal to a plane boundary in the plasma. One advantage of this method is that only the magnetic field vector on both sides of the boundary is needed, however, it only provides the direction of the normal vector and not the orientation, i.e. the normal gives the orthogonal to the boundary surface, but does not tell whether it is moving outward or inward.

As the aim of this paper is to determine the similarities and differences between the crossings of the diamagnetic cavity, a superposed epoch analysis (SEA; see Chree 1913) provides information on the uniformity of the different events by calculating an average cavity crossing. As the length of the event varies widely, we scale the signatures in time to an arbitrary time, with the point of entry and exit into/out of the field-free region fixed. With this scaling, the general structure of the magnetic field is preserved, however information on the timing is lost.

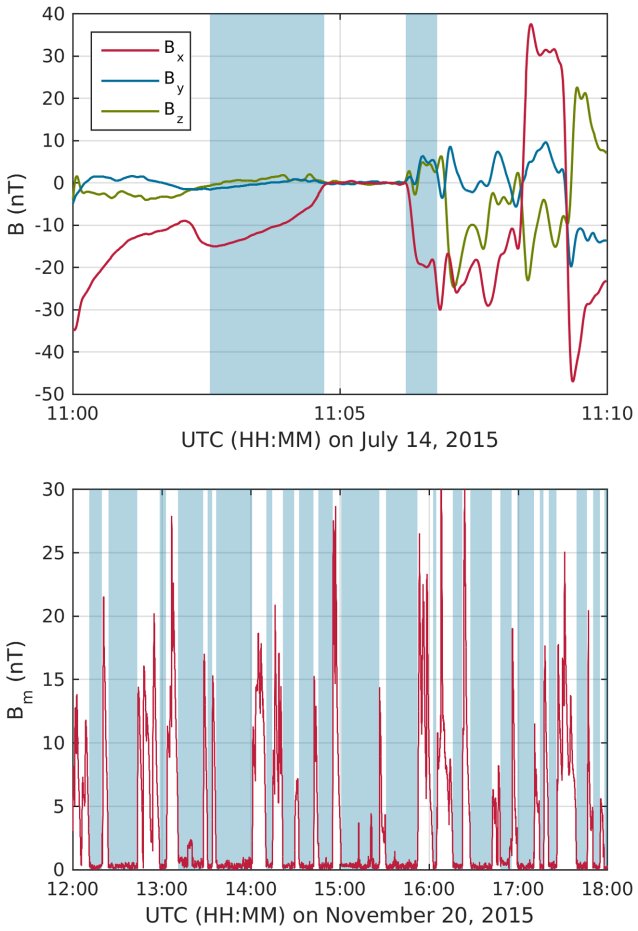

Figure 1. Two examples of RPC-MAG measurements around the cavity. The top panel shows a single event on 2015 July 14 with the boundary area marked in blue. This event is 1 min and 32 s long and is characteristic for many single events. The measurements shown in the bottom panel were made on 2015 November 20 and show several cavity crossings in quick succession interspersed with high magnetic field magnitude intervals. The zero-field regions are marked in blue. There are several days where this clustering can be observed.

3 INTERPRETATION

3.1 Magnetic field features

A total of 665 intervals when RPC-MAG registered the low field magnitudes combined with a lack of turbulence were determined, including estimates of the length of the transition regions. The individual intervals are listed in the Appendix. In total, *Rosetta* spent an accumulated time of 42 h in the cavity. The events are sorted into two groups: single events and clusters. Fig. 1 shows an example of the two groups. In the top panel the magnetic field components for a 10-min interval on 2015 July 14 are shown. First the field is almost entirely in x-direction, but then all components drop to zero. This marks the entry into the diamagnetic cavity. Afterwards the magnitude increases again and now the field direction is fluctuating. In the bottom panel only the magnetic field magnitude is shown. The cavity intervals here are tens of minutes long and are interspersed with shorter intervals with non-zero field. *Rosetta* enters the

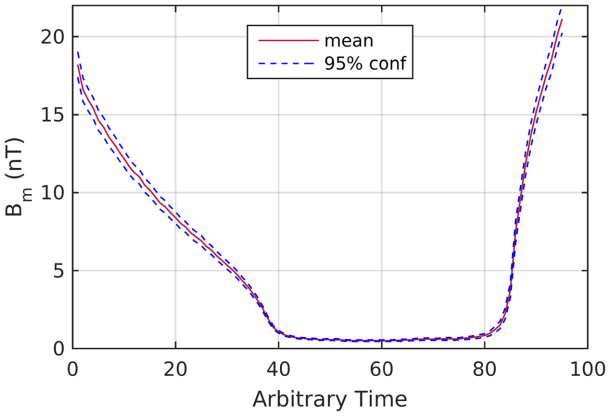

Figure 2. SEA of the magnetic field magnitude for all events (red) including the 95 per cent confidence interval in dashed blue lines.

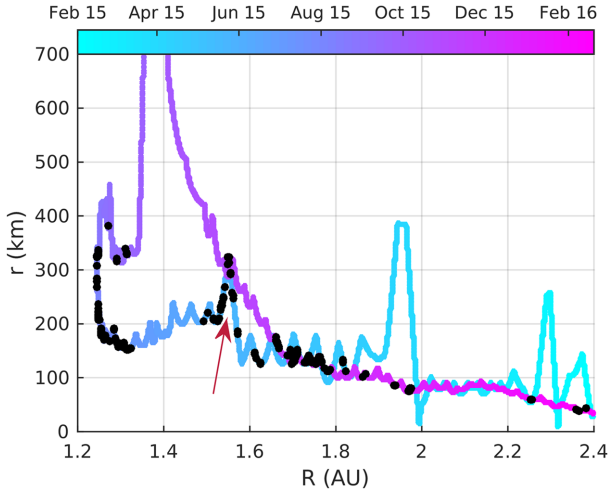

Figure 3. Rosetta's distance from the comet as a function of the distance of the comet to the Sun. The Colour scale indicates the time and the black dots mark the times that *Rosetta* is situated in the diamagnetic cavity. The arrow points to an unusual feature in mid to late May, where the extension of the cavity is unusually large.

cavity approximately every 55 min, but there is no stable frequency discernible for this interval. In general single events occur isolated from other cavities and may be as long as ∼30 min, they are always found in regions where the magnetic field is fluctuating heavily. Cluster events are defined as intervals where there are many cavity crossings right after each other. The magnetic field may increase between two events, but it typically does not reach the background field strength. In these intervals the field outside the cavity is generally also fluctuating without any apparent structure. So far the most prominent clusters were detected on 2015 July 30 and on 2015 November 19–21. Although they do occur every few minutes, there is no discernible frequency in the occurrence of clustered cavities.

The SEA of all events is shown in Fig. 2. Any features that may be seen in this analysis will be common features of most cavity crossings. First the magnetic field decreases from 20 to 5 nT, then the decrease steepens until the field is close to zero. In the cavity the field remains zero until a slight upward trend leads into the transition region where the magnetic field again increases to 20 nT. It is notable that the confidence interval of the mean cavity is very small, indicating that all cavity crossings are remarkably similar.

There are some other features that are common to most events. Because of *Rosetta* being mostly above the day–night line of the comet, the magnetic field draping (Alfvén 1957) results in B_x being the dominant component in most cases. The dominant component also changes sign in 1/3 of all cases, as was also observed for a single case by Goetz et al. (2016). As indicated by the SEA the inbound pass (cavity expanding) is almost always longer by a factor of ∼3 than the outbound pass (cavity contracting). The mean duration of the inbound pass, the zero-field region and the outbound pass is 160 s : 230 s : 50 s. Although they do vary quite dramatically from 10 s : 8 s : 6 s to 17 min : 40 min : 24 min.

There is no correlation between low solar wind dynamic pressure/magnetic pressure and the cavity events. Although sometimes they coincide with low solar wind pressures, there are also events where a cavity is measurable and the solar wind dynamic pressure and magnetic pressure are elevated compared to normal levels. Consequently, low solar wind pressures cannot account for the large distance of the cavity boundary to the nucleus. A reversal in the solar wind magnetic field at the exact time that *Rosetta* is in the cavity could possibly account for the change in sign that is observed for some events. However from the observed common occurrence of the changes in magnetic field sign, we rule out the solar wind source of this feature. It should also be noted that solar wind data at the comet is not available and propagation models using Earth-based data are very limited in capability for most of the mission due to large angular distances between Earth and 67P.

3.2 Dynamical features

Fig. 3 shows *Rosetta*'s position and the comet's position as well as the intervals when *Rosetta* was located in the cavity. First of all, the size of the cavity increases with the comet's approach to the Sun, then after perihelion it increases further. This is due to a delay in the temporal development of the gas production rate, which was still increasing for 2–3 weeks after closest approach. The highest recorded extension of the cavity was on 2015 September 3 at 380 km. Afterwards *Rosetta* increased its distance to the comet significantly and no cavities were detected until mid-November when 67P was at a distance of 1.65 AU from the Sun. Then, the cavity distances are approximately the same as they were on the comet's inbound trajectory, although they are detectable at lower altitudes than before.

There is also an unusual feature (marked by an arrow) in late May, when the cavity distance seems to increase by a factor of 1.5–2 above its usual value. This feature is not related to any obvious change in the plasma environment of the comet, the solar wind or the outgassing rate. Also, no indication of significantly elevated neutral gas densities was observed. It is also not related to the position of the spacecraft with respect to the comet or the Sun. However, this phenomenon coincides with the spring equinox at 67P. At this time the outgassing profile shifts from peaking in the Northern hemisphere to the Southern hemisphere (Hansen 2016). This shift may relate to the cavity boundary distance, however the exact mechanism needs to be studied in more detail.

To search for a relationship of the gas production rate Q with the distance of the cavity r_c from the nucleus, we use the H_2O gas production rate model by Hansen (2016). This model depends on the comet's distance from the Sun R and gives two dependences, one before perihelion, one after:

$$Q = 1.32 \times 10^{28}\, R^{-4.62} \quad \text{for } t \le t_{\rm ph}, \tag{2}$$

$$Q = 8.72 \times 10^{28}\, R^{-5.71} \quad \text{for } t > t_{\rm ph}, \tag{3}$$

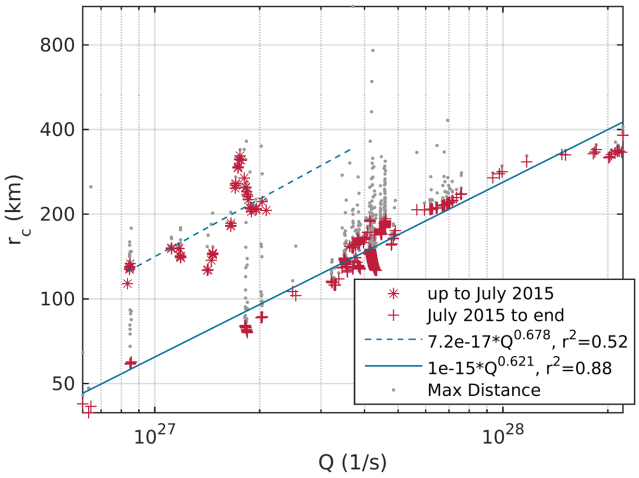

Figure 4. Cavity boundary distance over the empirical gas production rate. The events are clearly grouped: stars indicate the event took place before 2015 July, crosses indicate events from 2015 July to 2016 February. The blue lines show the corresponding linear fit and the fit parameters are given in the legend. The grey dots give an estimate of the maximum extension of the cavity while *Rosetta* is located in this region and cannot observe the boundary.

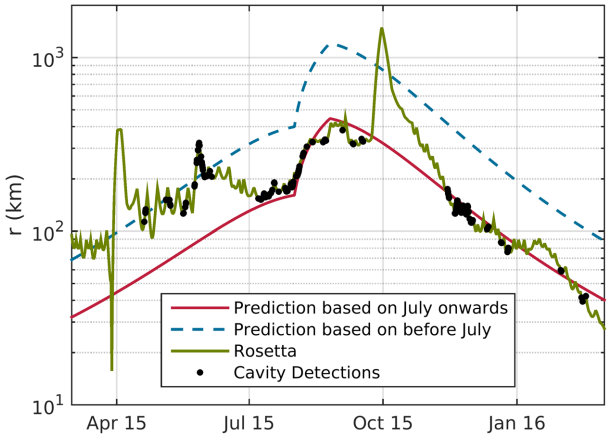

Figure 5. Prediction of cavity distance based on the relationship between gas production rate and distance. The red line corresponds to equation (5) and the blue dashed line to equation (4). *Rosetta*'s trajectory is shown in green and the actual detections of the cavity are indicated by black points. The time interval shown here is truncated from March 15 to March 16, because the cavity has only been detected in that time interval.

where t_{ph} is the time of perihelion passage (2015 August 13) and R is measured in astronomical units. As this model displays a step at perihelion, we apply a smoothing average of 50 points to the model to smooth out the step.

Fig. 4 shows the cavity detection distances as a function of the gas production rate. There are clearly two different populations: one before 2015 July 1 and one after. This is in accordance with the anomaly around equinox. Because of these populations we choose to fit these events separately. The prediction of the cavity distance r_c (km) to the comet is

$$r_c = 7.2 \times 10^{-17}\, Q^{0.678} \quad \text{for } t < 2015\,\text{July}, \tag{4}$$

$$r_c = 1.0 \times 10^{-15}\, Q^{0.621} \quad \text{for } t \geq 2015\,\text{July}. \tag{5}$$

The r^2 values for these fits are 0.52 and 0.88, respectively. The exponent is also very close to an analytical value given by Cravens (1987), who derived a dependence of the contact surface on the production rate to be $Q^{0.75}\,\text{cm}^{-1}$. However we would not expect the above relationships to match the analytical expression exactly as the magnetic field and electron density radial profile they use is not the same as the one we observe with *Rosetta*.

Additionally the analytical model also shows that the distance depends on the magnetic field as $r_c \propto 1/B$, where B is the maximum magnetic field strength in the pile-up region. This relationship is difficult to investigate as the field in the pile-up region is highly variable as described previously. If we assume that the average magnetic field in the pile-up region is the mean field in the hour before the cavity event, we can recreate Fig. 4 and find that the exponent for R in equation (5) is 0.8. However the estimate of the field is heavily skewed towards zero for multiple crossings which skews the entire population. Therefore this estimate can only provide a reference. However, the exponent also matches the analytical model quite well.

It should be noted that the distance we use here is only exact in the moment the cavity boundary moves over *Rosetta*. During the times that *Rosetta* is in the cavity it may expand further. This can be estimated using the velocity estimates as explained below and the duration of zero field measurements. The result is indicated in grey in Fig. 4. This may partially fill the gap between the populations, however it should be noted that this estimate is based on many assumptions. For example, we assume that the expansion speed of the cavity is constant, which is unlikely. Therefore, we do not incorporate these points into our fit.

Additionally the spread of the measurements of r_c at a certain gas production rate may be due to an unstable boundary. This would mean that the fit we have presented here does not indicate the actual global cavity distance, but is instead the cavity distance as an overlap of the global cavity and possible instabilities/anomalies.

In a second step the above fit may be used to predict the cavity distance for the whole interval from 2015 March to 2016 March. Fig. 5 shows the predictions for the cavity distance and *Rosetta*'s trajectory along with the actual detections of a cavity. Clearly the prediction based on the cavity events from April–June is not correct at other times, if it were, *Rosetta* would be in the diamagnetic cavity for almost the entire mission. In contrast, the red curve seems to fit well. During the close flyby in 2015 March, the cavity does not seem to be formed yet (Koenders 2016, this issue), otherwise it should have been detected using either prediction. This should also be the case for late February, where *Rosetta* went sufficiently close to the nucleus to be able to detect a cavity. Because this was not the case, we infer that the cavity was no longer present at that time.

The gas production rate used here is only valid for H_2O, so it stands to reason that the discrepancy between the two fits may be caused by significant contributions of other species. Except for water the most abundant species is CO_2. Fougere et al. (2016) present calculations for the ratio between the CO_2 gas production rate and the H_2O gas production rate for 2015 May 6, which is in the time interval that shows elevated distances for the cavity. They find that the ratio is 0.04–0.05, meaning water is still by far the dominating species. A composition of 5 per cent CO_2 and 95 per cent H_2O would result in a 5 per cent higher ion–neutral drag. This is insignificant compared to what would be needed to push out the cavity to where it is measured.

Additionally it should be noted that with the new model for the gas production rate the peak value increased to $Q_{max} = 4 \times 10^{28}$ which is significantly higher than what was assumed in

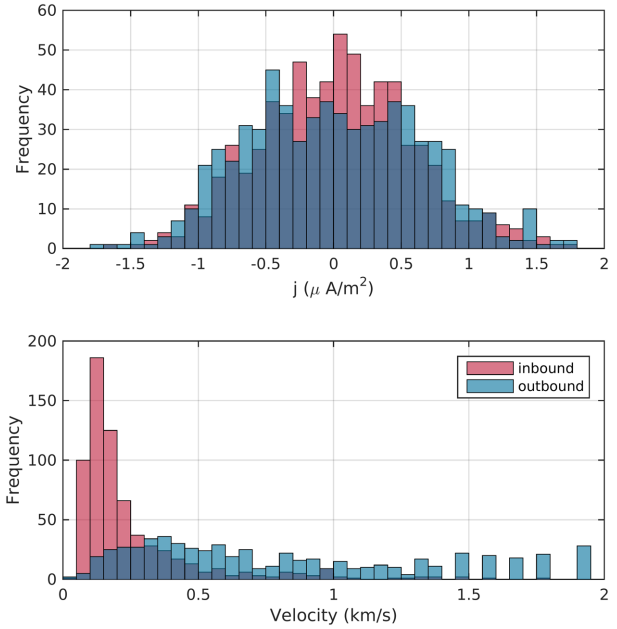

Figure 6. Histogram of the calculated current in the boundary region (top) and the velocity of the boundary (bottom) for the inbound and outbound pass separately. For both calculations the boundary is assumed to be 25 km in width.

simulations and models up until now. For example the gas production rate in the simulations by Koenders et al. (2015) is assumed to be $Q_{\max} = 5 \times 10^{27}$, which in Fig. 4 corresponds to a diamagnetic cavity distance from data of 180 km. This is still significantly larger than the predicted 50 km, however the difference is only a factor of ∼3.6 instead of a factor of ∼7.6.

So far there has been no correlation between outbursts as seen by OSIRIS and the detection of a cavity. This assessment is based on the major outburst listed by Vincent et al. (2016) and a visual inspection of one time interval with many cavities as well as dense OSIRIS imaging cadence, aiming to correlate cavity times also fainter transient events.

If we assume a cavity boundary thickness of $L \approx 25$ km as calculated for 1P/Halley by Neubauer (1988), and for 67P in simulations by Rubin et al. (2012) and Koenders et al. (2015), it is possible to calculate the current density at the boundary:

$$\mu_0 |j| = |\nabla \times B| \approx \frac{|B|}{L}, \tag{6}$$

where L is the characteristic length scale. The results vary widely for the crossings (Fig. 6, top panel). The values for the current density are of the order of 1 μA m^{-2}, which is close to the current density determined from AMPTE magnetic field measurements for the boundary of the artificial cavity (Luehr et al. 1988). As the current depends on the peak magnetic field only and not on the duration, the inbound and outbound crossings follow the same general profile. This is not the case for the velocity of the boundary (Fig. 6, bottom panel), which was estimated using the transition time and a transition region thickness corresponding to L. Because of the very short transition time on the outbound pass, the velocity is highly variable and large in this case, especially when compared to the lower velocity and smaller spread of the inbound pass. The mean velocities and standard deviations are 260 (270) m s^{-1} inbound and 950 (710) m s^{-1} outbound.

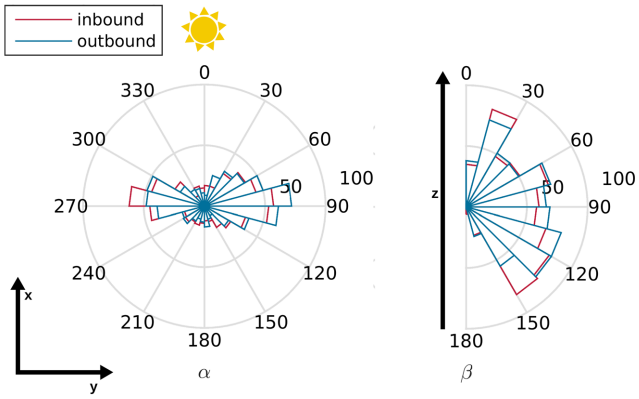

Figure 7. Minimum variance direction angle histogram in the x–y and x–$y_\perp$ plane (CSEQ). The Sun is indicated in yellow. This histogram does not take into account the position of the nucleus and is centred at *Rosetta*.

3.3 Shape of the diamagnetic cavity

The shape of the cavity may be inferred from the normal to the cavity boundary. However it should be noted that the cavity is probably not stable and will vary greatly over the time interval from 2015 April to 2016 February. Nonetheless the distribution of the normal vector is used to infer the cavity shape. This approach has the advantage of being entirely independent of the actual position of the spacecraft around the comet and therefore should exclude the influence of the gas production rate. Fig. 7 shows the histogram of the angle α and β of the normal vectors, which are the angles in the x–y plane and the angle to the positive z-axis, respectively. The vectors were determined by the MVA for the inbound and outbound transitions. The distribution of α is heavily skewed towards 90°. The second peak at 270° belongs to the same group, as the MVA does not yield the orientation of the vector and therefore there are two possible angles in the x–y plane for each individual case. There is no significant difference between inbound and outbound, which indicates that the boundary moving over *Rosetta* does not change direction and therefore is most probably the same one on the inbound and outbound pass.

The angle β behaves differently, in the 15°–150° range there is an almost uniform distribution for both inbound and outbound normal vectors. There are significant deviations from this uniform distribution only at 0° and 180°, meaning there are no normal vectors along the direction of the z-axis. Neither α nor β depend on the position of the spacecraft, meaning there is no correlation between the angles and the spacecraft phase angle, clock angle or distance to the comet.

To discuss this distribution and implications on the shape of the cavity, we first assume that the cavity is roughly ellipsoidal or paraboloidal, as it was done in previous studies at comet 1P/Halley and as shown as case 1 in Fig. 8. Then almost all normal vectors should lie in the y–z plane as *Rosetta* is in a terminator orbit ($x = 0$ km) for most of the time. This case only matches our results if there are small disturbances on top of the global shape as suggested by Neubauer (1987). Then the angle α has a similar distribution as the one we present here. Furthermore, the distribution of β should be dependent on the location of *Rosetta* and approximately be the same for all values between 0° and 180°. This is not observable here. The correlation coefficient between β and the polar angle of *Rosetta's* position is 0.02, meaning there is no correlation. This shows that a strictly ellipsoidal or paraboloidal global cavity surrounding the nucleus as shown as case 1 in Fig. 8 is not supported by the data.

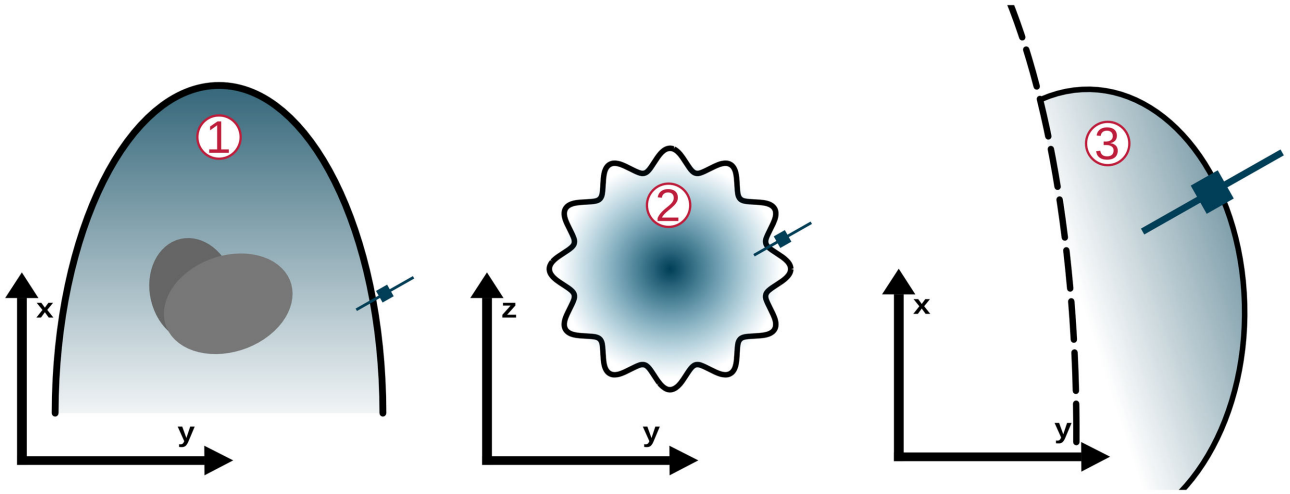

Figure 8. Schematic of the three discussed possibilities for the shape of the cavity. Case 1 and 3 are in the x–y plane and case 2 is a cross-section for $x = 0$ in the y–z plane. In the sketch for case 3 a possibly connected global cavity is alluded to by black dashed lines.

We therefore conclude that the cavity that is observed at 67P is not the global, stable cavity that was crossed at 1P/Halley.

If we still assume that the cavity observed here is a global structure we must consider another case. In this case the global cavity is extended by longitudinally fluted surface undulations as illustrated as case 2 in Fig. 8. In this case it is difficult to differentiate this model from others, as the direction of the angle β should follow a normal distribution. However one fact makes this case unlikely: if these ripples are distributed on an underlying ellipsoid shape then the angle α should change significantly when *Rosetta* is located in front ($x > 0$ km) of the comet. This is not the case with the data. This means that at least a uniformly distributed longitudinal oscillation on a global cavity is unlikely.

Based on our previous study we assume that the cavity boundary crossing are due to *Rosetta* passing strong undulations of the cavity boundary. These undulations cause pockets of plasma into which are moving over *Rosetta* causing it to enter and leave the field-free region on short time-scales. To derive an approximate description of these pockets we tried several different structures. For example, we assumed a longitudinally sinusoidal shape of the undulations and determined the resulting distributions of the boundary normal vectors. No suitable fit was found. Next, we assumed half-circle undulations. Such undulations did not agree with the measured distributions for α and β either. The best match was derived for an ellipsoidal-like structure, that is small ellipsoids attached to the global cavity boundary as sketched in Fig. 8, case 3. We therefore fitted an ellipse to the normal vectors. Because the normal fitting method would require the position of the normal vectors, which we cannot use as it varies with the outgassing rate, we adopted a slightly different approach. First a reference ellipse with its semimajor axis parallel to the x-axis and using a certain ellipticity is constructed. Then, an angle distribution of the normal vector is calculated and compared with the distribution from the data. The final result is the ellipse where the distributions have the highest correlation coefficient. The distributions are shown in Fig. 9. In this case the ellipse has an eccentricity of $e = 0.87 \pm 0.2$ with correlation coefficients greater than 0.85. This means that the semimajor axes have a ratio of about 1: 2. Varying the orientation of the semimajor axis does not result in a better fit. It should also be noted that fitting only one half of the ellipse does not change the results as the MVA does not give the direction of the normal. This study takes into account all 665

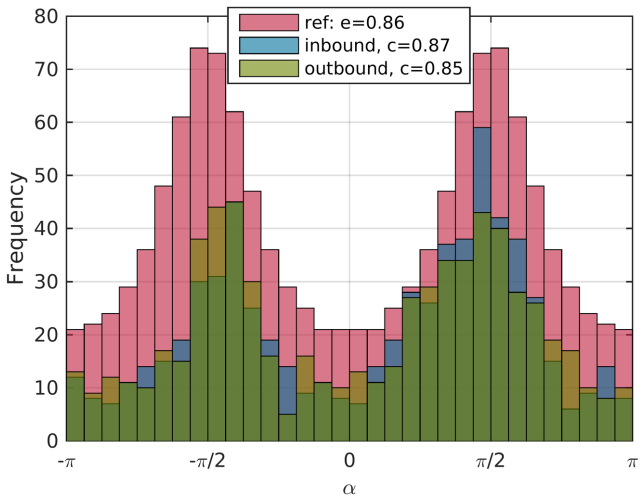

Figure 9. Angle distribution for the angle α for the inbound (blue) and the outbound (green) pass compared to the corresponding angle distribution of the reference ellipse that has the highest correlation with the measured angle distribution (red).

events, if we divide the events into summer (before 2015 October) and winter (after 2015 October) and perform a similar analysis, the ellipse is a better fit for the former interval than it is for the latter. This may indicate that the cavity boundary is more unstable then, which may be related to the lower outgassing rate during that time.

This means the instability deforms the boundary to form roughly elliptically shaped field-free pockets that may extend far from the global cavity as shown in Goetz et al. (2016). In this case, the shape that was calculated here is just the shape of the surface wave and not the shape of the cavity itself. With this model it is also possible to estimate the wavelength of the undulation. From the elliptical fit we know that the semimajor axes have a ratio of 1: 2. Therefore the wavelength should be two times the radial extension of the fitted ellipse. As described in the next section the curvature radius (which is equal to the semiminor axis) is around tens of kilometres. Thus the wavelength should be in the low hundreds of kilometres.

When fitting the ellipse we also cannot rule out that the field-free region is indeed ellipsoidal in shape and not connected to

a larger structure at all. There are two possible mechanisms to explain an isolated cavity: first of all, these pockets may actually be caused by the spacecraft itself. In this case the neutral gas and ion densities in this spacecraft cavity should be elevated far above normal levels. This may be due to spacecraft rotations that cause sublimation (Schläppi et al. 2010) or due to thruster firings. But data from ROSINA show no elevated neutral gas density, RPC does not measure elevated ion counts and there is no correlation with thruster firings. We therefore rule out this possibility.

Second, these pockets could be 'minicavities' caused by passing boulders. As seen by OSIRIS these boulders are of sizes up to 50 m on the surface (Pajola et al. 2015) and 0.8 m detached from the surface (Fulle et al. 2016) and have an outgassing rate of their own. If such a boulder produces enough neutral gas, this may be able to push out the magnetic field in a small region around the boulder. However, as before, we would then expect a significant neutral gas density increase in the cavity, which is not the case. To affirm this supposition we can estimate the size of a cavity produced by a point source with the same outgassing rate as a spherical boulder with a diameter of 10 m. The outgassing rate of the boulder is estimated by scaling it with the surface area. If we assume an outgassing rate of 10^{28} s^{-1} for the nucleus, which has a surface area of $\sim$40 km^2, the outgassing rate of the boulder (area of $\sim$300 m^2) is about 8×10^{22} s^{-1}. The radial profile of the neutral gas close to the source is (Haser 1957)

$$n_\mathrm{n} = \frac{Q}{4\pi u_\mathrm{n} r^2}, \tag{7}$$

and with equation (1) we get

$$r_\mathrm{c}^2 = \frac{n_\mathrm{i} m_\mathrm{i} k_\mathrm{in} Q \mu_0 L}{2\pi B^2}. \tag{8}$$

In this expression the radial derivative has been substituted by a characteristic length scale L that depends on the thickness of the transition region. If we assume water ions with a density of 1000 cm^{-3} and a magnetic field of 20 nT, which are average values at perihelion, the only unknown is the characteristic length scale. If L is set to a high value of 10 m, the radius of the cavity is 5 m. This is smaller than the diameter of the boulder, but even considering this as a height above the surface *Rosetta* would have to pass within metres of such an object for the cavity to be detected. This has not been observed during the entire mission and boulders with a diameter of 10 m have not been observed so far at comet 67P. In contrast to that the cavity was detected in numerous instances. It is highly unlikely that boulders would pass close to the spacecraft that frequently and be missed by the remote sensing instruments. We therefore conclude that boulders ejected from the comet are not the source of the field-free region that RPC-MAG detected.

4 CONCLUSION

We have analysed RPC-MAG data to find all indications of diamagnetic cavity detections over the entire *Rosetta* mission. The resulting 665 events have been analysed to determine the properties of the cavity and its boundary. There are two distinct groups of cavity events, single and clustered, that seem to be randomly distributed, but there is no discernible frequency in the clustered events, and there is no explanation as to why the cavity is present more often on certain days. The distance of the cavity boundary to the nucleus depends on long-term trends in the outgassing rate but is not related to the rotation rate or short time variations like outbursts. We find that for events after spring equinox the distance r_c is related to the outgassing rate as $r_\mathrm{c} \propto Q^{0.6}$. All boundary crossings show remarkably similar magnetic field features, they are embedded in a magnetically highly variable region, when the magnetic field decreases slowly to zero and then increases, on average, five times faster than the decrease. In 1/3 of all cases the magnetic field changes sign during the cavity. There is no evidence that the cavity is only detected when the solar wind pressure is low.

A MVA reveals that the cavity boundary may roughly be described by an ellipse in the x–y plane, however it is found that this ellipse is not centred on the comet, as the boundary normal distribution does not match a global cavity especially in the perpendicular plane. The boundary velocity was estimated to be of the order of 1 km s^{-1} and the current density is about 1 μA m^{-2}.

All evidence points to the fact that the cavity observed at 67P is not entirely the global structure as seen at 1P/Halley but small pockets of zero magnetic field. Two explanations, a 'minicavity' due to a passing boulder and a spacecraft produced cavity, has been ruled out. However, the instabilities that were proposed by Goetz et al. (2016) fit the data. In this case we would neither expect the pressures to be equal at the boundary nor the normal vector to be dependent on the measurement.

Based on these discussions, the formation of instabilities at the cavity boundary and a higher than expected outgassing rate is the most likely explanation for the unusual behaviour of the diamagnetic cavity at 67P.

ACKNOWLEDGEMENTS

The RPC-MAG and ROSINA data will be made available through the PSA archive of ESA and the PDS archive of NASA. *Rosetta* is a European Space Agency (ESA) mission with contributions from its member states and the National Aeronautics and Space Administration (NASA). The work on RPC-MAG was financially supported by the German Ministerium für Wirtschaft und Energie and the Deutsches Zentrum für Luft- und Raumfahrt under contract 50QP 1401. The work on ROSINA was funded by the federal state of Bern, the Swiss National Science Foundation and the ESA PRODEX program. Work at LPC2E/CNRS was supported by CNES and by ANR under the financial agreement ANR-15-CE31-0009-01. Portions of this research were performed at the Jet Propulsion Laboratory, California Institute of Technology, under contract with NASA. We are indebted to the whole of the *Rosetta* Mission Team, SGS and RMOC for their outstanding efforts in making this mission possible. We acknowledge the staff of CDDP and IC for the use of AMDA and the RPC Quicklook data base (provided by a collaboration between the Centre de Données de la Physique des Plasmas, supported by CNRS, CNES, Observatoire de Paris and Université Paul Sabatier, Toulouse and Imperial College London, supported by the UK Science and Technology Facilities Council).

REFERENCES

Alfvén H., 1957, Tellus, 9, 92
Auster H.-U. et al., 2015, Science, 349, 015102
Balsiger H. et al., 2007, Space Sci. Rev., 128, 745
Biermann L., Brosowski B., Schmidt H. U., 1967, Sol. Phys., 1, 254
Chree C., 1913, Philos. Trans. R. Soc. Lond. Seri. A, 212, 75
Cravens T. E., 1987, Adv. Space Res., 7, 147
Eriksson A. I. et al., 2007, Space Sci. Rev., 128, 729
Fougere N. et al., 2016, A&A, 588, A134
Fulle M. et al., 2016, ApJ, 821, 19
Glassmeier K.-H. et al., 2007, Space Sci. Rev., 128, 649

Goetz C. et al., 2016, A&A, 588, A24
Gombosi T. I., De Zeeuw D. L., Häberli R. M., Powell K. G., 1996, J. Geophys. Res., 101, 15233
Haerendel G., 1987, Geophys. Res. Lett., 14, 673
Haerendel G., Paschmann G., Baumjohann W., Carlson C. W., 1986, Nature, 320, 720
Hansen K. C., 2016, MNRAS, 00, 00
Haser L., 1957, Bull. Soc. R. Sci. Liege, 43, 740
Huang Z. et al., 2016, J. Geophys. Res. (Space Phys.), 121, 4247
Ip W.-H., Axford W. I., 1987, Nature, 325, 418
Keller H. U. et al., 2007, Space Sci. Rev., 128, 433
Koenders C., 2016, MNRAS, 462, S235
Koenders C., Glassmeier K.-H., Richter I., Ranocha H., Motschmann U., 2015, Planet. Space Sci., 105, 101
Luehr H., Kloecker N., Acuna M. H., 1988, Adv. Space Res., 8, 11
Nemeth Z. et al., 2016, MNRAS, 462, S415
Neubauer F. M., 1987, A&A, 187, 73
Neubauer F. M., 1988, J. Geophys. Res., 93, 7272
Neubauer F. M. et al., 1986, Nature, 321, 352
Pajola M. et al., 2015, A&A, 583, A37
Rubin M., Hansen K. C., Combi M. R., Daldorff L. K. S., Gombosi T. I., Tenishev V. M., 2012, J. Geophys. Res. (Space Phys.), 117, 6227
Schläppi B. et al., 2010, J. Geophys. Res. (Space Phys.), 115, A12313
Sonnerup B. U. O., Cahill L. J., Jr, 1967, J. Geophys. Res., 72, 171
Szegö K. et al., 2000, Space Sci. Rev., 94, 429
Tao C., Kataoka R., Fukunishi H., Takahashi Y., Yokoyama T., 2005, J. Geophys. Res. (Space Phys.), 110, 11208
Trotignon J. G. et al., 2007, Space Sci. Rev., 128, 713
Tsurutani B. T., Smith E. J., 1986, Geophys. Res. Lett., 13, 263
Vincent J.-B. et al., 2016, MNRAS, 462, S184

SUPPORTING INFORMATION

Supplementary data are available at *MNRAS* online.

cavity_times.txt

Please note: Oxford University Press is not responsible for the content or functionality of any supporting materials supplied by the authors. Any queries (other than missing material) should be directed to the corresponding author for the article.

This paper has been typeset from a TEX/LATEX file prepared by the author.